Review

Journal of the Ceramic Society of Japan 114 [1] 26–35 (2006)

External-Field Hot-Water Treatments of Sol–Gel Derived SiO_2–TiO_2 Coatings for Surface Nanostructure Control

——A Review——

Atsunori MATSUDA, Mototsugu SAKAI, Toshihiro KOGURE,*
Kiyoharu TADANAGA** and Masahiro TATSUMISAGO**

Department of Materials Science, Toyohashi University of Technology, 1–1, Hibarigaoka, Tempaku-cho, Toyohashi-shi, Aichi 441–8580
**Department of Earth and Planetary Sciences, Graduate School of Science, The University of Tokyo, 7–3–1, Hongo, Bunkyo-ku, Tokyo 113–0033*
***Department of Applied Chemistry, Graduate School of Engineering, Osaka Prefecture University, Gakuen-cho, Sakai-shi, Osaka 599–8531*

外部場温水処理によるゾル–ゲル SiO_2–TiO_2 系コーティング膜の表面ナノ構造制御（総説）

松田厚範・逆井基次・小暮敏博*・忠永清治**・辰巳砂昌弘**

豊橋技術科学大学物質工学系，441–8580 愛知県豊橋市天伯町雲雀ヶ丘 1–1
*東京大学大学院理学系研究科地球惑星科学専攻，113–0033 東京都文京区本郷 7–3–1
**大阪府立大学大学院工学研究科応用化学分野，599–8531 堺市学園町 1–1

This review paper is focused on the area of titania nanocoatings prepared from sol–gel derived films by hot-water treatment under external reaction fields to design their functionality through the control of their surface morphology and crystallinity at low processing temperatures. First, the formation of titania nanocrystalline coatings at low temperatures by wet chemical procedures is briefly reviewed. Second, a concept of material design based on an external-field hot-water treatment for sol–gel derived films and the effects of the external fields on the formation of titania nanocrystals from the sol–gel derived films are discussed. Finally, promising characteristics of the resultant titania nanocrystal-dispersed coatings with unique morphology are described. External fileds of vibrations and electric voltages affect the nanostructure of titania crystallites formed on SiO_2–TiO_2 gel coatings during hot-water treatment. Without the external fields granular anatase nanocrystals of 30–50 nm in size are formed on the coatings during the hot-water treatment, whereas the shape of the precipitates becomes sheetlike by applying a vibration to the substrate during hot-water treatment. Similar changes in shape of the precipitates on the coatings are also observed, and ramiform (branchlike) crystallites are formed at the negative electrode by applying an electric field between the substrates. The sheetlike and ramiform crystallites are mainly composed of a hydrated titania, $m(TiO_2)\cdot nH_2O$, with the lepidocrocite-like layered structure with a d-spacing of 0.6–0.8 nm. Titania nanosheets are characterized by a large surface-to-volume ratio, which gives rise to the excellent wettability for water and antifogging properties. Processing temperatures for the preparation of the coatings are lower than 100°C under atmospheric pressure, so that the coatings have a great potential for applications to various substrates including organic polymers with poor heat resistance.

[Received September 21, 2005; Accepted November 17, 2005]

Key-words : *External field, Sol–gel coating, Hot-water treatment, Titania, Nanosheet, Nanocrystal*

1. Introduction

SOL–GEL processing is a wet chemical route for the preparation of glasses, ceramics, inorganic–organic hybrids and nanocomposites from alkoxide-derived colloidal suspensions.[1),2)] Sol–gel processing offers many advantages such as low process temperatures, production of highly pure, homogeneous materials and the design of pore size-controlled porous materials. Through sol–gel processing, monoliths, fibers, particles and coatings can be obtained from the colloidal suspensions. Among them, the formation of coatings is recognized as a promising application from the practical point of view, since coatings can be formed on various substrates such as glass, metal and plastic with a large surface area and nonflat geometry. The process is cost-effective in comparison with conventional vacuum coating techniques such as sputtering and chemical vapor deposition. The sol–gel functional coatings and their applications reported range, for example, from optical, chemical, mechanical and ferroelectronic coatings to micropatterning, electrochromic devices, photocatalysts, and biomedical applications.

The discovery by Fujishima and Honda of water splitting with a titania photoanode led to a wide variety of photoelectrochemical applications.[3)] For instance, titania-based coatings have attracted much attention as photocatalysts in the decomposition of environmental pollutants, photoinduced superhydrophilic coatings, self-cleaning coatings, and electrodes for dye-sensitized photochemical solar cells.[4)–12)] The control of the nanostructures of the titania-based coatings further offers an exciting opportunity to enhance their unique physical and chemical properties. The performance of their photocatalytic reactions depends on the characteristics of the titania cryatallites, such as the size and surface area. Titania nanocrystals show higher photocatalytic activities than the bulk, since the nanosized crystals have a large surface area per unit mass which facilitates the diffusion of excited electrons and holes towards the surface before their recombination. A high dispersion of the nanocrystals in the host matrix without aggregation is also important to enhance the activity. A large surface area, high transmittance of UV light, and durability against photocatalytic activity are required for the host matrix

in which the nanocrystals are dispersed. Silica gel is a candidate matrix for meeting these requirements. Therefore, several kinds of silica-titania nanocomposite coatings have been studied for photocatalytic, superhydrophilic and self-cleaning applications.

The sol–gel method is a promising technique for fabricating the titania nanocoatings of interest here. However, high-temperature processing is generally required to form nanocrystals in the coatings. For example, a heat treatment at temperatures higher than 300°C is necessary to form titania crystallites from homogenous, amorphous pure TiO_2 gel films and much higher temperatures of around 1000°C are needed for the crystallization for SiO_2–TiO_2 gel films containing smaller amounts of TiO_2. Thus, lowering of process temperatures for crystallization and control of the shape and phase of the crystallites are required to design the functionalities of the advanced titania-based nanocoatings by the sol–gel method. Over the past years, lowering of processing temperatures to form titania coatings with high crystallinity has been extensively studied because of the need to use organic polymer substrates that have poor thermal stability. We have reported that anatase TiO_2 is formed in sol–gel derived $83.5SiO_2 \cdot 16.5TiO_2$ by exposure to an environment of high temperature and high humidity.[13] The structural changes of the SiO_2–TiO_2 coatings proceed as follows: (1) dissociation of Si–O–Ti bonds in the coating by the attack of water vapor, (2) formation of Ti–O–Ti bonds, and (3) nucleation and growth of anatase TiO_2. The addition of an organic polymer, such as polyethylene glycol (PEG), makes the resultant coating porous after heat treatment due to the thermal decomposition of PEG. This allows the formation of anatase nanocrystals not only at the surface but also inside the coatings. Imai and coworkers reported the formation of anatase in TiO_2 gel films by exposure to water vapor at 60–180°C using an autoclave, while heat treatments at higher than 400°C are required for crystallization in a dry atmosphere.[14),15)] The exposed TiO_2 films become brittle with a decrease in the concentration of OH groups. They proposed an important mechanism wherein water vapor attacks strained bonds and induces a cleavage of the bonds through hydrolysis and a rearrangement of the network. More recently, Langlet et al. autoclaved TiO_2 gel films at 90–140°C under various water/ethanol atmospheres.[16)] Optimum crystallization was obtained for low water pressure in the range of 0.6–1.5 bar. Crystallization of TiO_2 gel film in an autoclave caused an increase in porosity, which reduced the abrasion resistance of the films. Anatase nanocrystallite films containing small amounts of the brookite phase have been prepared from PEG-containing titania gel films by a boiling-water treatment.[17)] The nanocrystallite films consisted of anatase crystallites with dimensions on the order of 5 nm and showed good electrochromic performance. Anatase crystalline titania coatings with a grain size of about 20 nm successfully formed on cotton fabrics at low temperatures by boiling-water treatment under ambient pressure have been reported.[18)] Such a titania coating on fabrics is promising for use as an antibacterial photocatalyst in the textile industry. Wu et al., reported that anatase of good crystallinity has been developed on Ti metal substrates by treating with H_2O_2 aqueous solution at 80°C followed by soaking in distilled water at ambient temperature, subsequent aging in distilled hot water at 80°C.[19)] The involvement of H_2O molecules in the atomic rearrangement is considered to lead to the amorphous-to-anatase transformation. The anatase layer exhibits good bioactivity for inducing apatite deposition in a simulated body fluid.

Several low-temperature crystallization processes, other than boiling-water treatment for alkoxide-derived titania gel films, have been reported. Deki and cowokers showed that anatase thin films were prepared from $(NH_4)_2TiF_6$ aqueous solution with added H_3BO_3 by a liquid phase deposition at room temperature.[20),21)] The formation of anatase is based on the chemical equilibrium reaction between the metal fluorocomplex ion and the metal oxide in the aqueous solution. The anatase crystallite size for the transparent film was estimated to be 5–10 nm for the as-deposited film, and it increased to about 20 nm after a heat treatment at 600°C. Ichinose et al. reported that anatase films were prepared from peroxotitanium acid solution and peroxo-modified anatase sol by heat treatment.[22),23)] For the crystallization of anatase, about 250°C is necessary for the films derived from the peroxotitanium acid solution, whereas no heat treatment is needed for the films derived from peroxo-modified anatase sols. The peroxo-modified anatase sols were originally prepared from peroxotitanium hydrate suspensions or peroxotitanium acid solutions with heating or autoclaving at about 100°C and have the advantages of nanosize arrowhead-like anatase precursors of high stability. Direct synthesis of rutile films on substrates at near room temperatures from $TiSO_4$ aqueous solution has been reported by Yamabi and Imai.[24),25)] The crystalline phase of titania is determined by the initial pH value and Ti concentration of the precursor solutions. The deposition rate dose not have a strong effect on the crystalline phase, whereas properties of anions as a ligand for Ti ions have a great influence on the morphology of the titania crystallites. An interesting evolution of a new morphology of films consisting of highly crystalline, rectangular parallelepiped rutile on the submicron scale has also been reported.[26)] The rutile films are synthesized via hydrothermal treatments of aqueous $TiCl_3$ solutions containing a large amount of NaCl at 200°C.

2. Concept for designing titania nanocoatings by external-field hot-water treatment of sol–gel films

We have shown that anatase nanocrystals are formed on sol–gel derived SiO_2–TiO_2 coatings upon hot water treatment at 97°C for 1 h, as well as water-vapor treatment.[27)–29)] In the hot-water treatment, substrates with coatings are immersed into hot, pure water and kept at rest for a given time. The formation of anatase nanocrystals is rarely observed in the pure TiO_2 coating under the same conditions. PEG added to the gel coating is completely leached out in about 1 min of the hot-water treatment. Anatase nanocrystals are formed mainly on the surface of the coating without the addition of PEG, whereas the addition of PEG allows the formation of anatase not only on the surface but also throughout the inside of the coating. This can be ascribed to the porous structure of the coating after the leaching of PEG. High photocatalytic activities of the anatase nanocrystal-dispersed coatings have been demonstrated by the decomposition and oxidation of acetaldehyde, NO*x*, methylene blue, and potassium iodide.[30)–32)] Although it takes a longer period of time, considerable amounts of anatase nanocrystals are formed on the SiO_2–TiO_2 coatings even at 38°C after a treatment of 65 h.[33)] The amounts of anatase nanocrystals formed by hot-water treatment are maximum for the SiO_2–TiO_2 coatings with TiO_2 contents of around 25 mol%.[34)] The resultant coating shows high photocatalytic activity and excellent wettability for water. The high concentration of Si–O–Ti bonds and the hydrolyzed sites should facilitate the nucleation and growth of anatase nanocrystals.

Anatase nanocrystal-dispersed coatings can be formed on plastic substrates such as poly(ethylene terephralate), acrylic

resin and polycarbonate.[35] The plastic substrates with coatings obtained without PEG show good weathering resistance owing to the protective effects of the residual silica-rich underlayer. In addition, hydrophobic and photocatalytically active surfaces have been successfully prepared using micropatterned anatase nanocrystal-dispersed coating and fluoroalkylsilane vapor deposition.[36]

The control of the nanostructures of the titania-based coatings further offers an exciting opportunity to enhance their unique physical and chemical properties. The control of the shape and phase of the titania crystallites, as well as lowering of process temperatures for crystallization, is required to design the functionalities of the advanced titania-based nanocoatings by the sol–gel method. Anatase formation in sol–gel derived SiO_2–TiO_2 coatings during hot-water treatment proceeds through the hydrolysis of Si–O–Ti bonds, dissolution of the SiO_2 component, migration of hydrolyzed titania species, and nucleation and growth of TiO_2. The SiO_2–TiO_2 coatings are porous and have a large specific surface area, so that the gel coatings can easily react with water molecules in a very short time. The hydrolysis, dissolution and recrystallization are influenced not only by the physicochemical conditions such as temperature, pressure and pH of the solution, but also by external vector fields such as vibration, electric field, magnetic field, etc. The concept of designing the titania nanocoatings by an external-field hot-water treatment of sol–gel derived multicomponent films is illustrated in **Fig. 1**. Water flow driven by vibration of the substrate is expected to change the collision rate between water molecules and the gel films and to induce a gradient in the concentration of hydrolyzed species. The hydrolyzed species exhibits an intrinsic surface charge in the solution. Therefore, electric field and magnetic field, as well as vibration, should influence the hydrolysis, dissolution and recrystallization of the gel films. Applying the above concept, i.e., design of materials by external-field hot-water treatment of sol–gel derived multicomponent films, we recently demonstrated that the shape of the precipitates elongated into nanosheets of hydrated titania upon applying vibration to the substrate during the treatment.[37),38] It was also found that the shape of the precipitates on the coating at the negative electrode changed from granular to ramiform upon applying an electric field to the substrates during the treatment.[39] In the following sections, the new findings that sheetlike and ramiform titania nanocrystals are formed on SiO_2–TiO_2 gel coatings by hot-water treatment under external vector fields, such as vibration and electric voltage, are described in detail. The similarities and differences in the formation of sheetlike and ramiform titania nanocrystals are discussed.

3. Advanced coatings prepared by external-field hot-water treatment and their characterization

3.1 Preparation of coatings by sol–gel process

The chemical composition of $75SiO_2 \cdot 25TiO_2$ (mol%) was selected for the starting gel films to compare the effect of the external fields on the formation of titania nanocrystals since the amounts of titania precipitated in the films during hot-water treatment are maximized at this composition.[34] Coating films were formed on various kinds of substrates by dipping withdrawing in ambient atmosphere. The preparation procedure is the same as reported in the literature.[37)–39] Silicon tetraethoxide and titanium tetra-*n*-butoxide were used as the starting materials. Ethanol and hydrochloric acid are the solvent and catalyst, respectively. The substrates with the SiO_2–TiO_2 coatings were dried at 90°C for 1 h in air. Non-alkali glass plates (NA35, NH Techno Glass), silica glass

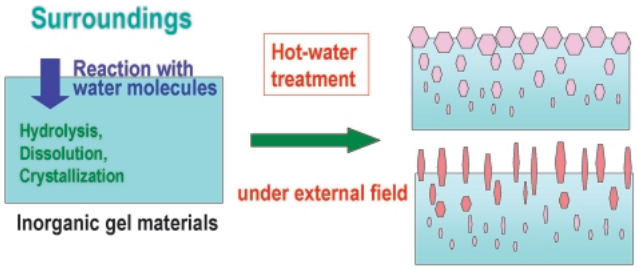

Fig. 1. Concept for design of titania nanocoatings by external-field hot-water treatment of sol–gel derived multicomponent films.

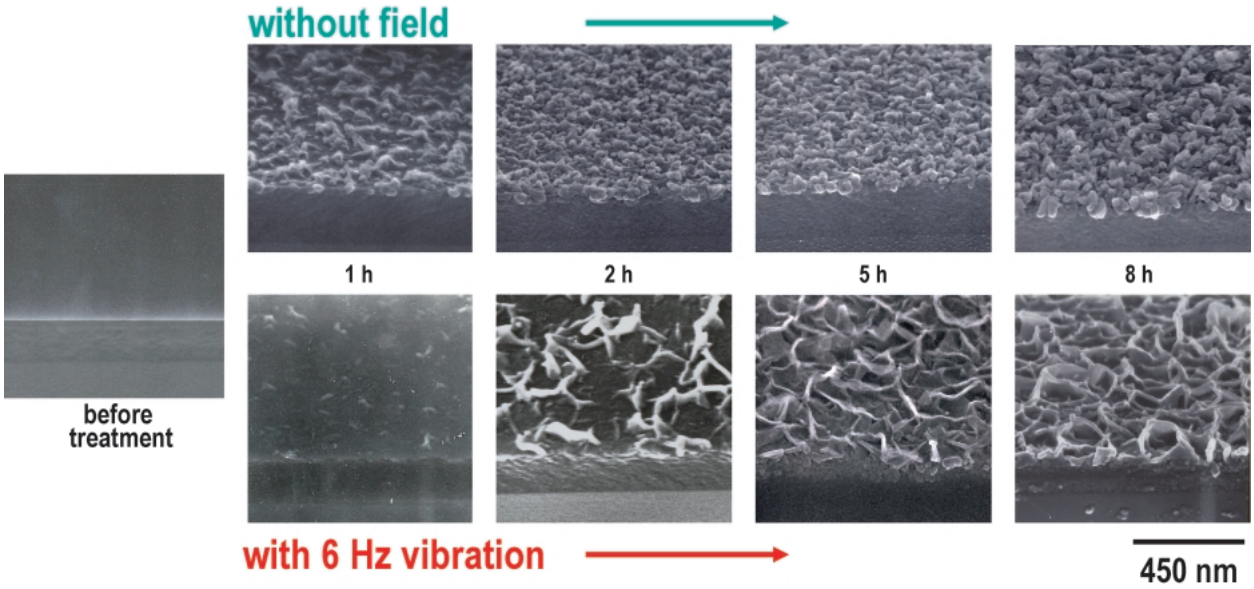

Fig. 2. SEM images of the formation of granular anatase without vibration (upper row) and nanosheet precipitates with vibration of approximately 6 Hz (lower stand) during the hot-water treatment at 90°C.

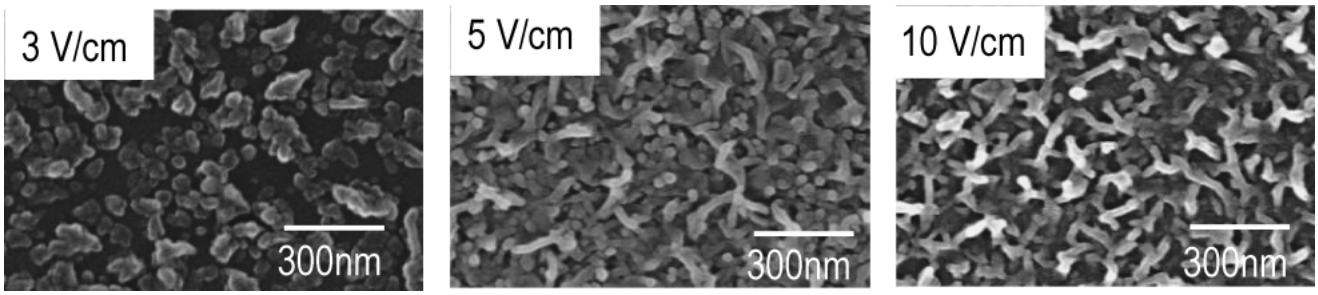

Fig. 3. SEM images of the surface of the coatings at the negative electrodes treated with hot water of 90°C for 5 h under various electric fields.

plates (Sumikin Ceramics & Quartz), indium tin oxide (ITO)-coated glass plates (Nippon Sheet Glass) and silicon wafers (Mitsubishi Sumitomo Silicon) were used as the substrates.

3.2 External-field hot-water treatment of coatings

In the case of vibration hot-water treatment, the substrates with coatings were immersed into 300 ml of hot water at 90°C with vibration of 0 to 25 Hz with an amplitude of 2.5 mm. A handmade apparatus consisting of a clip shaft, a transducer, a variable resistor and a direct-current power source was used to apply a given vibration to the substrate.

With regard to electric field hot-water treatment, a pair of ITO substrates coated with the SiO_2–TiO_2 coating were placed in hot water at 90°C and then a DC voltage of 0 to 10 V was applied between the substrates which were facing each other at a distance of 1 cm.

3.3 Characterization of coatings

The changes in the texture of the coatings during hot-water treatment were examined using a field-emission scanning electron microscope (FE–SEM, Model S–4500, Hitachi). The structures of the coatings and precipitates were identified using a field-emission transmission electron microscope (FE–TEM, Model HF–2000, Hitachi), equipped with an energy dispersive X-ray spectrometer (EDS, Sigma, Kevex). Electron-transparent specimens for the TEM examination were prepared using Ar ion milling. The thermal stability and phase transition of coatings were also examined using SEM and TEM. The average roughness and surface profile of the coatings were evaluated using an atomic force microscope (AFM, Nanopics, Seiko Instruments). The thickness of the coatings was mainly evaluated using a surface profilometer (TDA–22, Kosaka Laboratory).

Fourier-transformed infrared (FTIR) absorption spectra of the coatings on silicon substrates were measured in the transmission mode using FT–IR1650, Perkin–Elmer. Chemical analyses for the composition of the coatings were carried out by X-ray photoelectron spectroscopy (ESCA–K1, Shimadzu). Ultraviolet-visible (UV-Vis) transmission spectra of silica glass or non-alkali glass substrates, one side of which was coated with a film, were obtained using V–560, JASCO.

Changes in the contact angle of water on the coatings with UV light irradiation were measured using a contact angle meter (CA–C, Kyowa Surface Science). Photocatalytic activities of the coatings were evaluated from the results of photobleaching of methylene blue (MB) aqueous solutions and the amounts of photogenerated I_2 in potassium iodide (KI) aqueous solutions during UV irradiation.

4. Formation of sheetlike and ramiform precipitates on coatings

Granular, anatase precipitates are formed on the SiO_2–TiO_2 coatings by hot-water treatment at 90°C without vibration, whereas the shape of the precipitates elongates by applying vibration to the substrate during the hot-water treatment. Longitudinal vibration is preferable for forming sheetlike precipitates compared with transverse vibration. The shape of the precipitates clearly becomes nanosheet-like upon hot-water treatment with longitudinal vibration of ca. 6 Hz. However, the amount of the nanosheet precipitate decreases with longitudinal vibration of ca. 10 Hz and almost no precipitates are formed above ca. 12.5 Hz. Typical SEM images of the formation of sheetlike precipitates with vibration of ca. 6 Hz during the hot-water treatment are shown in the lower image of **Fig. 2**. The formation of granular anatase without vibration is also shown in the upper image of Fig. 2 for comparison. It is clear that the shapes and growth rates of the precipitates differ depending on the conditions. With vibration, nanosheet precipitates are preferentially formed on the coating at a lower growth rate during hot-water treatment. Such a phenomenon in the formation of titania precipitates in the SiO_2–TiO_2 system upon hot-water treatment is not observed for the sol–gel derived pure TiO_2 coatings under the same conditions.

With respect to the effect of the electric field, the shape of the precipitates at the negative electrode changes from granular to ramiform upon applying a DC voltage to the substrate during the hot-water treatment, while such changes in the shape of titanaia nanocrystals are not observed at the positive electrode. SEM images of the surface of the coatings at the negative electrodes after hot-water treatment at 90°C for 5 h under various electric fields are shown in **Fig. 3**. Granular precipitates grow to be ramiform and the precipitate concentration tends to decrease by applying an electric field of 3 Vcm^{-1}. When the electric field is 5 Vcm^{-1}, round and ramiform precipitates coexist. Ramiform precipitates become dominant and the shape becomes distinct when an electric field of 10 Vcm^{-1} was applied. The formation of ramiform precipitates upon electric-field hot-water treatment is also a unique phenomenon in the SiO_2–TiO_2 system, which is not observed for the sol–gel derived pure TiO_2 coatings.

SEM images of the precipitates formed on the coatings (a) without external fields, (b) with vibration of ca. 6 Hz and (c) with an electric field of 10 Vcm^{-1} after the hot-water treatment for 5 h are shown in **Fig. 4**. The shape of the titania precipitates is clearly influenced by the external field such as vibration and electric field. Sheetlike form is very distinct for the precipitates formed by vibration hot-water treatment. These results demonstrate that external-field hot-water treatment of multicomponent gel films is a promising method of fabricating functional nanocoatings with unique surface morphology.

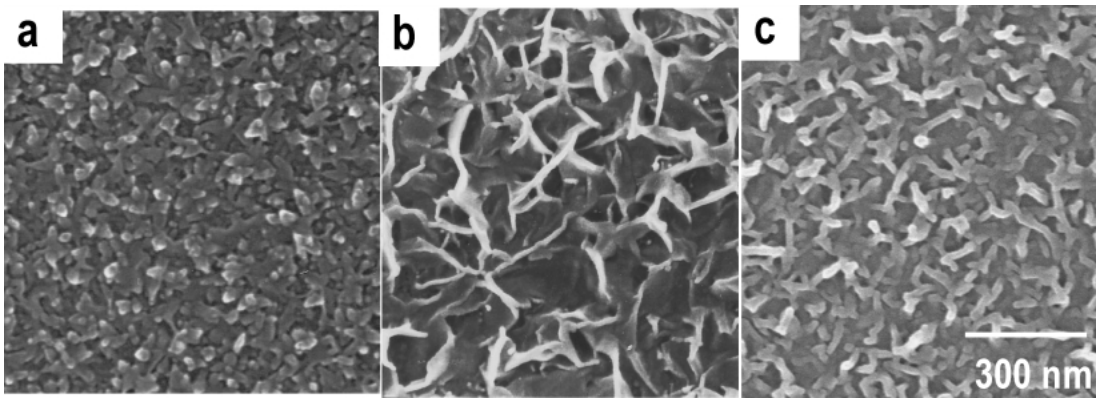

Fig. 4. SEM images of the precipitates formed on the coatings (a) without any external field, (b) with vibration of 6 Hz and (c) with electric field of 10 V/cm after the hot-water treatment at 90°C for 5 h.

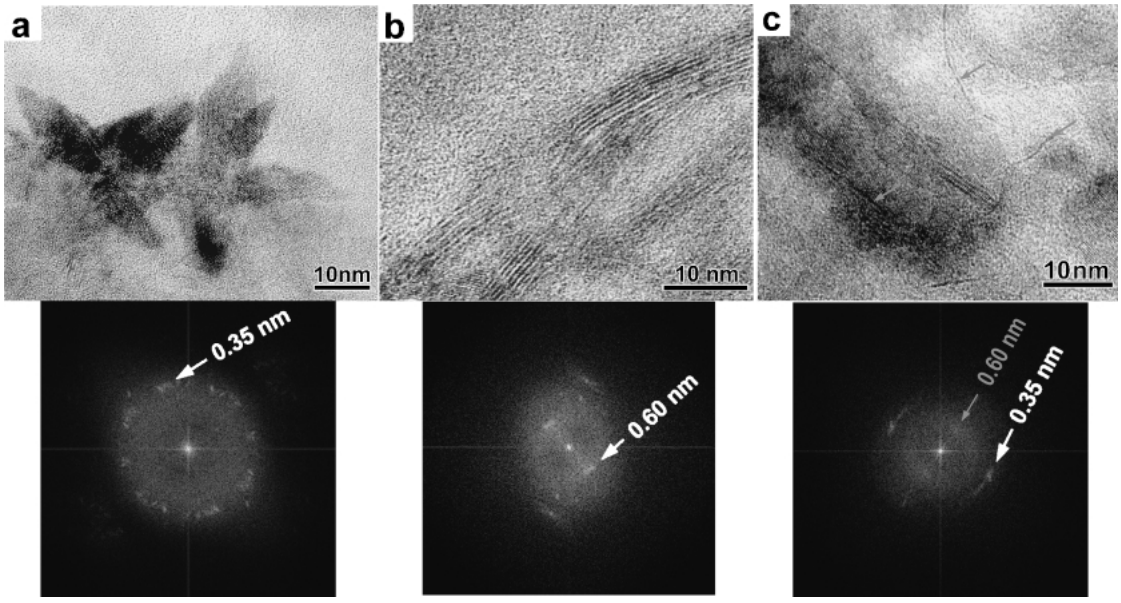

Fig. 5. HRTEM images and corresponding Fourier transform patterns of granular, sheetlike and ramiform precipitates. Preparation conditions of the precipitates are the same those described in Fig. 4.

5. Identification of sheetlike and ramiform precipitates on coatings

For the identification of the sheetlike and ramiform precipitates, plan-view high-resolution TEM images (HRTEM) of the specimens prepared by ion milling were obtained and compared with that of granular anatase precipitates formed on the coating with neither vibration nor electric field. The HRTEM images and corresponding Fourier transform patterns of granular, sheetlike and ramiform precipitates are shown in **Fig. 5**. Preparation conditions of the granular, sheetlike and ramiform precipitates are the same as for those in Fig. 4. Crystallites of approximately 30 nm with a lattice fringe of 0.35 nm corresponding to the lattice spacing of (101) in anatase are observed (Fig. 5a). Sheetlike crystallites of 100–200 nm length and less than 10 nm thickness are formed (Fig. 5b). The sheetlike crystallites consist of layers with a spacing of 0.6–0.63 nm and include layers with a spacing of around 0.8 nm. Spots corresponding to the lattice spacing of 0.6 nm are seen in the Fourier transform patterns. On the other hand, ramiform crystallites are generally less than 100 nm in length and about 10 nm in thickness (Fig. 5c). The round precipitates and sheetlike precipitates indicated by the arrows in Fig. 5c are observed, where two or three sheets with the spacing of (0.6 nm are identified. Spots corresponding to the lattice spacing of 0.35 nm, which is equivalent to the lattice spacing of (101) in anatase are seen in the Fourier transform patterns, whereas the spots corresponding to the lattice spacing of 0.6 nm of sheetlike precipitates (Fig. 5b) are not distinct. This is probably due to the high dispersion of sheetlike nanocrystals as a monolayer. The difference in crystalline shapes between granular, sheetlike and ramiform nanocrystals formed by hot-water treatment is confirmed from these HRTEM images and Fourier transform patterns.

Electron diffraction patterns from anatase and titania nanosheet are shown in **Fig. 6**. Anatase and titainia nanosheet represent the granular precipitates obtained without external field and the sheetlike precipitates obtained with vibration during hot-water treatment, respectively. The observed diffraction pattern from the anatase nanocrystals agrees well with the calculated one. On the other hand, the pattern from

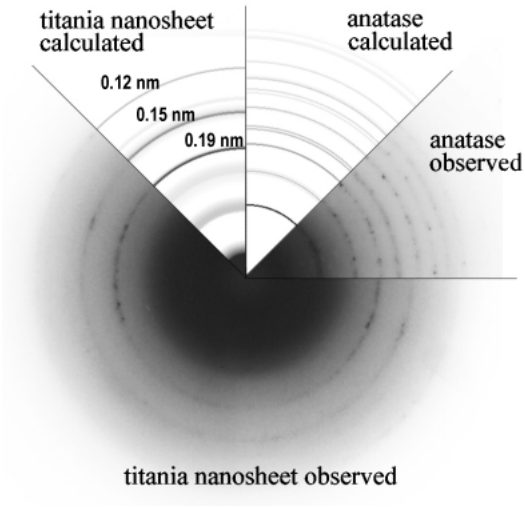

Fig. 6. Electron diffraction pattern from the titania nanosheets obtained with vibrations of approximately 6 Hz (Bottom). Diffraction pattern from the anatase nanocrystals obtained without vibrations (Right). The calculated pattern, Debye–Scherrer rings, for anatase is also shown for comparison (Top right). The calculated pattern for the randomly oriented monolayers of hydrated titania with the lepidocrocite-like structure (Top left).

the titania nanosheets, which is characterized by three distinctive Deby–Scherrer rings corresponding to 0.19, 0.15 and 0.12 nm, is different from that of anatase, indicating that the crystalline phase of the titania nanosheet differs from anatase. Recently, Sasaki and coworkers reported a hydrated titania nanosheet with a lepidocrocite-like layered structure.[40),41)] The calculated diffraction pattern, using the Debye equation,[42)] from randomly oriented monolayers with this lepidocrocite-like structure is shown at the top left in Fig. 6. The three Debye–Scherrer rings in the pattern observed from the nanosheets are well reproduced. Therefore, it is concluded that the nanosheet consists of hydrated titania such as $m(TiO_2)\cdot nH_2O$ with the lepidocrocite-like layered structure. With regard to the identification of ramiform precipitates obtained by electric-field hot-water treatment, the ramiform precipitate consists of both anatase and isolated hydrated titaina with the lepidocrocite-like layered structure.

It has been reported that hydrated titania with a spacing between 0.6 to 0.9 nm can be prepared by ion exchange between protons and alkali ions in alkali titanate, such as $Na_2Ti_3O_7$, $K_2Ti_4O_9$ or $Cs_2Ti_5O_{11}$ obtained by a flux method at high temperatures around 1000°C using titanium dioxide and the corresponding alkali carbonate.[43)–48)] Regarding hydrated titania nanosheets, Sasaki and coworkers report the synthesis of nanosheets through exfoliation and delamination of hydrated titania flakes obtained through ion exchange.[45),46)] However, hydrated titania nanosheet-precipitated coatings obtained by the hot-water treatment with external fields have a unique surface topography. This type of unique coating with nanosheet precipitates is not obtained through conventional sol–gel processes based on the heat treatment of gel coatings from the sols.

6. Formation mechanism of sheetlike and ramiform precipitates

The formation mechanism of titania nanocrystals in the gel films with hot-water treatment is fundamentally very important. Tadanaga and coworkers have proposed a dissolution-reprecipitation mechanism for the crystallization of pseudoboehmite (γ-AlOOH) from Al_2O_3 gel films upon hot-water treatment. Al_2O_3 gel films dissolve in water and the pseudoboehmite nanocrystals are precipitated. Distinct rapid morphological changes in the surface, reflecting crystal habits, during hot-water treatment are reported. Unidirectinal growth of precipitates and the resultant flowerlike structure are similar to the formation process of hydrated titania and anatase.[49)–53)]

Penn and Banfield present an oriented attachment mechanism for crystal growth and the formation of dislocations for natural iron oxyhydroxide (FeOOH) minerals and highly ordered titania nanocrystallites.[54)–56)] In a natural system, crystals are generally considered to grow upon the addition of individual atoms and ions or the dissolution of unstable phases followed by reprecipitation of a more stable phase. However, iron oxyhydroxide crystals, for example, grow via an oriented attachment mechanism in which adjacent 2- to 3-nm-diameter particles aggregate and rotate such that their structures adopt parallel orientations in three dimensions. Long chains of highly ordered titania are obtained from a solution of sol–gel derived anatase nanoparticles under hydrothermal conditions. Under hydrothermal conditions, rapid growth of anatase particles occurs along [001], driven in part by the relatively high surface energy of (001) and in part by a kinetic effect involving a cyclic generation of highly reactive adsorption sites. Juggling of nanoparticles by Brownian motion allows adjacent particles to rotate into the low-energy configuration represented by a coherent particle-particle interface. In aggregation-based growth, reduction of surface free energy is achieved by the complete removal of pairs of surfaces.

Kavan et al.[57)] and another research groups[26),58),59)] reported the preparation of TiO_2 films on electrodes by anodic oxidative hydrolysis of $TiCl_3$. They proposed the formation of Ti (IV) oxo species in $TiCl_3$ aqueous solutions by anodic oxidation under hydrothermal conditions.

Grimes et al. reported a magnetically driven method for controlling nanodimensional porosity in sol–gel derived metal oxide films such as TiO_2, Al_2O_3 and SnO_2 coated on ferromagnetic substrates.[60)] The process involves the attraction of the moving charged sol particles to the out-of-plane magnetization vector of the substrate's domain walls through the associated Lorentz force, thereby replicating the domain wall structure of the substrate in the deposited metal oxide film.

The proposed mechanism of titania nanocrystal growth on SiO_2–TiO_2 coatings with hot water in the present work is as follows: (i) hydrolysis of Si–O–Ti bonds and dissolution of the SiO_2 component, (ii) migration of hydrolyzed titania species from the interior to the surface of the coating, and (iii) nucleation and growth of anatase nanocrystals at the surface of the residual coating. IR absorption spectra showed that applying vibration during hot-water treatment dose not accelerates hydrolysis of Si–O–Ti bonds or dissolution of the SiO_2 component. Therefore, the formation of anatase nanoparticles and hydrated titania is dominated not by the hydrolysis of Si–O–Ti bonds or the dissolution of the SiO_2 component but by nucleation and growth of hydrolyzed titania species at the surface of the coating. Rapid water flow driven by vibrations probably increases the collision rate between the gel coating and water molecules, and lowers the surface concentration of hydrolyzed titania species. This facilitates the formation of nanocrystals that include proton, hydroxyl and oxonium ions in their structure, which should prevent the formation of anatase or the transformation from

hydrated titanate to anatase, and allows the growth of hydrated titania into nanosheets. The chemical state and size of the hydrolyzed titania species are still not clear, however the orientation by the oriented attachment mechanism that was seen in titania nanocrystals is not observed for anatase and hydrated titania generated from the titania species under hot-water treatment. Anatase precipitates form on the SiO_2–TiO_2 coatings containing different amounts of TiO_2, i.e., 9, 16.5 and 33 mol%, during hot-water treatment without external field. Thus the enhanced interaction between hydrolyzed titania species and water due to the vibration is considered to have a greater influence on the formation of titania nanosheets than the chemical composition of the coatings.

Ramiform precipitates formed by the electric-field hot-water treatment contain considerable amounts of hydrated titania having a layered structure. Therefore, an electric field should allow hydrolyzed titania species to preferentially form hydrated titania on the SiO_2–TiO_2 gel coatings at the negative electrode. This phenomenon is analogous to that observed on the coating with hot-water treatment with vibration of the substrate. In the case of the vibration hot-water treatment, the formation of nanosheet-like hydrated titania is probably achieved by the lowering of the concentration of hydrolyzed titania species at the surface of the coating due to rapid water flow driven by the vibration. The detailed mechanisms of the formation of ramiform precipitates under an electric field are still not clarified, whereas the electrostatic repulsion between the hydrolyzed, negatively charged titania species[61),62)] and the negative electrode may lower the concentration of titania species at the surface of the coating and hence permit the preferential formation of hydrated titania and the ramiform structure. Another important factor to be discussed is the effects of redox at the electrodes and the higher pH of the hot water in the vicinity of the electrode; i.e., OH^- is generated from water near the negative electrode. Further detailed electrochemical analyses of the electric-field hot-water treatment of SiO_2–TiO_2 gel coatings are required. The identification of hydrolyzed titania species is important.

The above phenomena demonstrate that the crystalline phase and the morphology of nanocrystal-dispersed materials can be controlled by treating sol–gel derived multicomponent gels with hot water with external vector fields such as vibration and electric voltage. It is a low temperature, eco-friendly process and useful for creating advanced artificial coatings.

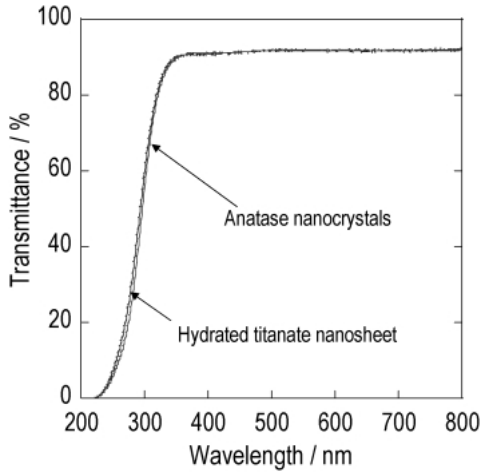

Fig. 7. Optical transmittance of granular anatase obtained without external fields and of sheetlike hydrated titania coatings obtained with vibration of approximately 6 Hz on silica glass substrates after hot-water treatment at 90°C for 5 h.

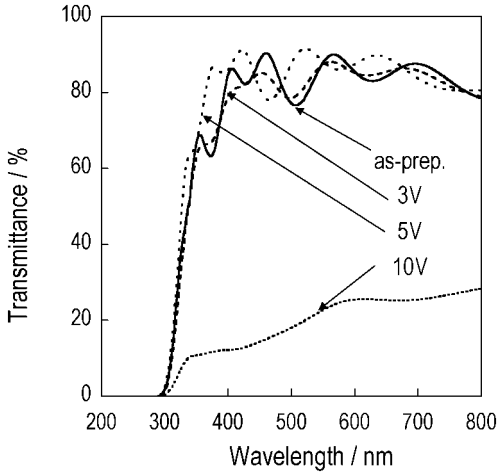

Fig. 8. Optical transmission spectra of the coatings on ITO-coated glass substrates used as a negative electrode after hot-water treatment at 90°C for 5 h under various electric fields.

7. Characterization of coating properties

Several important characteristics, such as transparency, photocatalytic activity, wettability for water and antifogging property, of titania nanocrystal-dispersed coatings are described in this section. **Figure 7** shows the optical transmittance of granular anatase obtained without external field and sheetlike hydrated titania coatings obtained with vibration of ca. 6 Hz on silica glass substrates after hot-water treatment at 90°C for 5 h. The transmittance of both coatings is as high as about 90% in the visible range including Fresnel's reflectance, indicating that the anatase nanocrystals and hydrated titania nanosheets cause no light scattering. The absorption edge is estimated to be about 360 nm for both coatings. Interference wavy patterns are very small, which means that the refractive index of the coatings almost matches that of the silica glass substrate due to large porosity at the surface of the coating and the presence of a silica-rich underlayer.

Figure 8 shows optical transmission spectra of the SiO_2–TiO_2 coatings on ITO-coated soda-lime glass substrates used as negative electrodes after hot-water treatment at 90°C for 5 h under various electric fields. The wavy patterns reflect the interference at the interfaces of air / SiO_2–TiO_2 coating / ITO coating / glass substrate. The ramiform shape of the titania precipitates becomes significant with increasing the applied voltage, and the coatings gradually become darker. The changes in the wavy patterns of the transmittance are caused by the changes in optical properties, such as refractive index and thickness, of the SiO_2–TiO_2 coatings during the hot-water treatment. The maxima, i.e., peak values, of transmission spectra of the coatings obtained by applying 3 and 5 Vcm^{-1} are as high as 90%, which is comparable to that of as-prepared coating. This indicates that the coatings treated under an electric field lower than 5 Vcm^{-1} is transparent independent of the formation of ramiform precipitates. On the other hand, the transmittance of the coating applied with 10 Vcm^{-1} is lower than 30% in the visible range. The colored coating obtained with 10 Vcm^{-1} becomes transparent after a heat treatment at 400°C in air. Therefore, the reduction from Ti^{4+} to Ti^{3+} in the coating causes the coloration of the coating. Drastic decreases

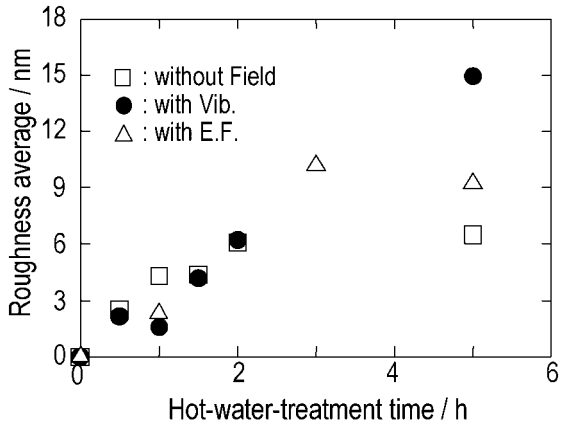

Fig. 9. Changes in average roughness of the SiO_2–TiO_2 coatings during the hot-water treatment. Open squares, closed circles and open triangles represent the treatment conditions without external field, with vibration of approximately 6 Hz, and with electric field of 5 Vcm^{-1}, respectively.

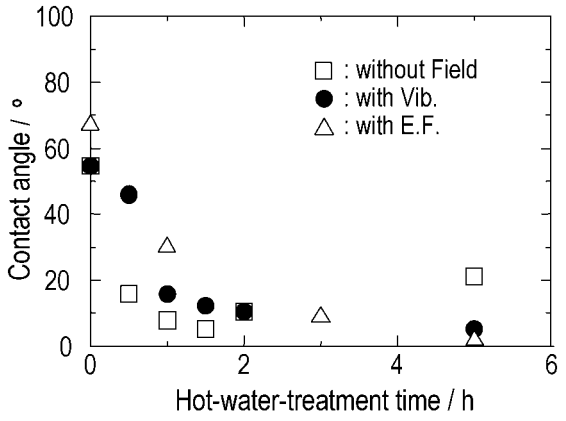

Fig. 10. Changes in contact angle for water of the SiO_2–TiO_2 coatings during hot-water treatment. Open squares, closed circles and open triangles denote the same conditions as those described in Fig. 9.

in transmittance at around 350 nm are due to intrinsic absorption bands of the SiO_2–TiO_2 coatings.

Changes in average roughness of the SiO_2–TiO_2 coatings during the hot-water treatment are shown in **Fig. 9**. Open squares, closed circles and open triangles represent the treatment conditions without external field, with vibration of ca. 6 Hz, and with electric field of 5 Vcm^{-1}, respectively. The surface roughness of all the coatings increases with treatment time. The average roughness of the coating without vibration tends to level off to about 7 nm over 2 h, whereas those of the coatings under the vibration and the electric field appear to be saturated at about 10 nm and 15 nm within 5 h, respectively. These surface roughness changes of the coatings correspond to the changes in surface morphology due to the formation of precipitates shown in Figs. 2–4. The coating obtained by the vibration hot-water treatment showed the highest roughness among the three kinds of coatings.

The wettability of solid surfaces with liquids is governed by the chemical property, i.e., surface energy, and the microstructure of the surfaces. For instance, fine roughness enhances the hydrophilicity and hydrophobicity of the solid surfaces. **Figure 10** shows changes in the contact angle for water of the SiO_2–TiO_2 coatings after hot-water treatment. Open squares, closed circles and open triangles denote the same conditions as described for Fig. 9. Before hot-water treatment, the contact angle for water of the coating was 55–68°. The contact angle decreases with treatment time under all conditions. This is caused by chemical and geometrical effects, that is, the increase in surface energy due to the elimination of residual organic groups and the formation of the very small roughness shown in Figs. 2–4. When the coating is treated with hot water without external fields, the contact angle for water of the coating decreases to a minimum after 1 to 2 h and then slightly increases during the treatment. The slight increase in contact angle implies that the chemical property of the surface has changed. SiO_2 is well known to show a lower contact angle for water, i.e., higher surface energy, than TiO_2, so that the SiO_2-rich underlayer may become covered with anatase nanocrystals. On the other hand, when the coating is treated with hot water under vibration or electric field, the contact angle gradually decreases and becomes less than 5° within 5 h of treatment time, which corresponds to the increase in surface roughness shown in Fig. 9. The surface of the underlayer is considered still to be incompletely covered with sheetlike or ramiform precipitates even after the treatment for 5 h.

Changes in contact angles for water of the coatings during storage in the dark under ambient atmosphere are of practical importance. In the dark, photocatalytic decomposition of organic adsorbates owing to titania is not expected, thus the contact angles for water of the titania coating increase due to the increase in the amounts of adsorbates on the coating as well as the structural changes of surface OH groups during storage. For instance, the contact angle for water of the pure anatase coating prepared by the conventional heat treatment at 500°C is about 40° and rapidly increases to about 80° over several days. On the other hand, titania nanocrystal-dispersed coatings obtained from SiO_2–TiO_2 coatings by hot-water treatment retain low contact angles for water during storage in the dark owing to the large roughness, and unique morphology as well as high surface energies of the hydrated titania and the silica-rich underlayer. For example, the sheetlike hydrated titania nanosheet-precipitated coatings retain good hydrophilicity even after storage in the dark for 2000 h.

High photocatalytic activities of granular anatase and sheetlike hydrated titania coatings obtained by the hot-water treatment without and with vibration are confirmed, whereas ramiform titania coatings obtained by the electric-field hot-water treatment show lower photocatalytic activities. The high photocatalytic activity of granular anatase and sheetlike hydrated titania coatings can be ascribed to the higher specific area as well as the good titania crystallinity. The lower activity of the ramiform titania coatings, in spite of the high specific surface area, is attributable to the presence of a small amount of Ti^{3+} ions or O^{2-} vacancies, which act as trapping sites for photoexcited electrons and holes.

A photograph of the antifogging properties of the coatings is presented in **Fig. 11**. Three kinds of glass substrates with coatings, which have been kept in the dark place 2000 h, are placed over hot water of 90–80°C. The samples have (a) pure anatase coating obtained from pure TiO_2 gel film by heat treatment at 500°C, (b) anatase nanocrystal-dispersed coating obtained by the hot-water treatment without external fields and (c) hydrated titania nanosheet coating obtained with vibration hot-water treatment. Among the three kinds of coatings, (c) is seen to show the best antifogging property, indicating the hydrated titania nanosheet-precipitated coatings to be versatile for applications in the field of optics as well as

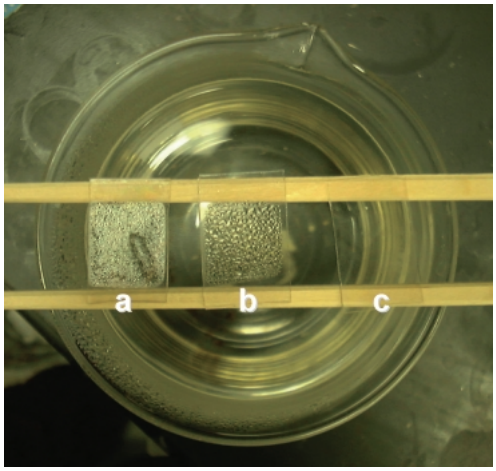

Fig. 11. Photograph of antifogging properties of the coatings holding over hot water at 80–90°C. Glass substrates have (a) pure anatase coating, (b) anatase nanocrystal-precipitated coating and (c) hydrated titania nanosheet-precipitated coating. This photograph was taken after the substrates with coatings had been kept in the dark in an ambient atmosphere for 2000 h.

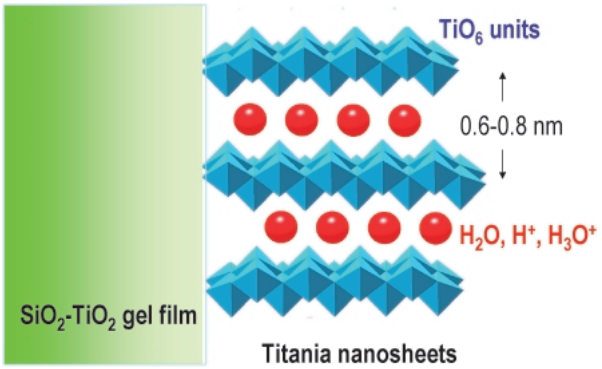

Fig. 12. Schematic illustration of the unique titania nanocoating obtained by external-field hot-water treatment for sol–gel derived SiO_2–TiO_2 films.

photocatalysts.

8. Summary and outlook

A concept of the material design based on external-field hot-water treatment for sol–gel derived films and the effects on the formation of titania nanocrystals from the films were discussed. Promising characteristics of the resultant titania nanocrystal-dispersed coatings with unique morphology were described. Unique coatings of sheetlike and ramiform titania nanocrystals with excellent wettability for water and antifogging properties were prepared by treating sol–gel derived SiO_2–TiO_2 films with hot water of 90°C under vibration and electric field. The titania nanocoating is schematically illustrated in **Fig. 12**. The sheetlike and ramiform titania precipitates include layers with a spacing of about 0.6 nm and were identified as hydrated titania with a lepidocrocite-type structure. The residual SiO_2–TiO_2 films have a composition gradient in the direction from the surface to the substrate due to the leaching of hydrolyzed titania species. The formation of sheetlike and ramiform titania precipitates is most likely due to the lowering of the concentration of hydrolyzed titania species at the surface by rapid water flow driven by the vibration or the electrostatic repulsion between the charged species and the electrode. Identification of hydrolyzed titania species, quantitative analysis of mass changes in the coatings during the external-field hot-water treatment, and electrochemical analysis are very important for clarifying the formation mechanism of the titania precipitates. In addition, the effects of other external fields, such as alternate current electric field, strong magnetic field and sonic field, on the formation of crystallites from gel films are also of interest. The new approach described here is a low temperature, eco-friendly process and provides a promising route for dramatically modification of the physicochemical properties and surface reactivity of nanocrystal-dispersed coatings.

Acknowledgements This work was partly supported by The Japan Society for the Promotion of Science (Grants-in-Aid for Scientific Research No. 15360344 (B) and No. 16360327 (B)), Nippon Sheet Glass Foundation for Materials Science and Engineering, Tatematsu Foundation, Izumi Science and Technology Foundation, and Hosokawa Powder Technology Foundation. The authors thank Professor Tsutomu Minami of Osaka Prefecture University for his continuous encouragement and guidance. They also thank all the students and graduate students in the Tatsumisago–Tadanaga Laboratory of Osaka Prefecture University, the Kogure Laboratory of The University of Tokyo, and the Sakai–Matsuda Laboratory of Toyohashi University of Technology for their technical assitance and cooperation.

References

1) Brinker, C. J. and Scherer, G. W., "Sol–Gel Science, The Physics and Chemistry of Sol–Gel Processing," Academic Press, New York (1990).
2) Sakka, S., "Handbook of Sol–Gel Science and Technology," Vols. I–III, Kluwer, Boston (2004).
3) Fujishima, A. and Honda, K., *Nature*, Vol. 238, pp. 37–38 (1972).
4) Mao, Y., Schoneich, C. and Asmus, K. D., "Photocatalytic Purification of Water and Air," Elsevier (1993) pp. 49–66.
5) Yamashita, H., Ichihashi, Y., Anpo, M., Hashimoto, M., Louis, C. and Che, M., *J. Phys. Chem.*, Vol. 100, pp. 16041–16044 (1966).
6) Choy, J., Park, J. and Yoon, J., *J. Phys. Chem. B*, Vol. 102, pp. 5991–5995 (1998).
7) Papoutsi, D., Lianos, P., Yianoulis, P. and Koutsoukos, P., *Langmuir*, Vol. 10, pp. 1684–1689 (1994).
8) Wang, R., Hashimoto, K., Fujishima, A., Chikuni, N., Kojima, E., Kitamura, A., Shimohigoshi, M. and Watanabe, T., *Nature*, Vol. 388, pp. 431–432 (1997).
9) Wang, R., Sasaki, N., Fujishima, A., Watanabe, T. and Hashimoto, K., *J. Phys. Chem. B*, Vol. 103, pp. 2188–2194 (1999).
10) Machida, M., Norimoto, K., Watanabe, T., Hashimoto, K. and Fujishima, A., *J. Mater. Sci.*, Vol. 34, pp. 2569–2574 (1999).
11) Hoffmann, M. R., Martin, S. T., Choi, W. and Bahnemann, D., *Chem. Rev.*, Vol. 95, pp. 69–96 (1995).
12) Linsebiger, A. L., Lu, G. and Yates, T., Jr., *Chem. Rev.*, Vol. 95, pp. 735–758 (1995).
13) Matsuda, A., Kogure, T., Matsuno, Y., Katayama, S., Tsuno, T., Tohge, N. and Minami, T., *J. Am. Ceram. Soc.*, Vol. 76, pp. 2899–2903 (1993).
14) Imai, H., Morimoto, H., Tominaga, A. and Hirashima, H., *J. Sol–Gel Sci. Technol.*, Vol. 10, pp. 45–54 (1997).
15) Imai, H. and Hirashima, H., *J. Am. Ceram. Soc.*, Vol. 82, pp. 2301–2304 (1999).
16) Langlet, M., Kim, A., Audier, M. and Herrmann, J. M., *J. Sol–Gel Sci. Technol.*, Vol. 25, pp. 223–234 (2002).
17) Djaoued, Y., Badilescu, S., Ashrit, P. V., Bersani, D., Lottici, P. P. and Bürning, R., *J. Sol–Gel Sci. Technol.*, Vol. 24, pp. 247–254 (2002).

18) Daoud, W. A. and Xin, J. H., *J. Am. Ceram. Soc.*, Vol. 87, pp. 953–955 (2004).
19) Wu, J., Hayakawa, S., Tsuru, K. and Osaka, A., *J. Ceram. Soc. Japan*, Vol. 110, pp. 78–80 (2002).
20) Deki, S., Aoi, Y., Hiroi, O. and Kajinami, A., *Chem. Lett.*, Vol. 1996, pp. 433–434 (1996).
21) Kishimoto, H., Takahama, K., Hashimoto, N. and Deki, S., *J. Mater. Chem.*, Vol. 8, pp. 2019–2024 (1998).
22) Ichinose, H., Terasaki, M. and Katsuki, H., *J. Ceram. Soc. Japan*, Vol. 104, pp. 715–718 (1996).
23) Ichinose, H., Terasaki, M. and Katsuki, H., *J. Sol-Gel Sci. Technol.*, Vol. 22, pp. 33–40 (2001).
24) Yamabi, S. and Imai, H., *Chem. Lett.*, Vol. 2001, pp. 220–221 (2001).
25) Yamabi, S. and Imai, H., *Chem. Mater.*, Vol. 14, pp. 609–614 (2002).
26) Hosono, E., Fujihara, S., Kakiuchi, K. and Imai, H., *J. Am. Chem. Soc.*, Vol. 126, pp. 7790–7791 (2004).
27) Matsuda, A., Kotani, Y., Kogure, T., Tatsumisago, M. and Minami, T., *J. Am. Ceram. Soc.*, Vol. 83, pp. 229–231 (2000).
28) Kotani, Y., Matsuda, A., Tatsumisago, M., Minami, T. and Kogure, T., *J. Sol-Gel Sci. Technol.*, Vol. 19, pp. 585–588 (2001).
29) Kotani, Y., Matsuda, A., Kogure, T., Tatsumisago, M. and Minami, T., *Chem. Mater.*, Vol. 13, pp. 2144–2149 (2001).
30) Matsuda, A., Kotani, Y., Kogure, T., Tatsumisago, M. and Minami, T., *J. Sol-Gel Sci. Technol.*, Vol. 22, pp. 41–46 (2001).
31) Kotani, Y., Matsuda, A., Matoda, T., Kogure, T., Tatsumisago, M. and Minami, T., *J. Mater. Chem.*, Vol. 11, pp. 2045–2048 (2001).
32) Matsuda, A., Matoda, T., Kotani, Y., Kogure, T., Tatsumisago, M. and Minami, T., *J. Sol-Gel Sci. Technol.*, Vol. 26, pp. 517–521 (2003).
33) Matsuda, A., Matoda, T., Tadanaga, K., Tatsumisago, M., Minami, T. and Kogure, T., *J. Am. Ceram. Soc.*, Vol. 88, pp. 1421–1426 (2005).
34) Matsuda, A., Matoda, T., Kogure, T., Tadanaga, K., Tatsumisago, M. and Minami, T., *J. Mater. Res.*, Vol. 20, pp. 256–263 (2005).
35) Matsuda, A., Matoda, Y., Kogure, T., Tadanaga, K., Minami, T. and Tatsumisago, M., *J. Sol-Gel Sci. Technol.*, Vol. 27, pp. 61–69 (2003).
36) Kobayashi, K., Matsuda, A., Kogure, T., Tadanaga, K., Minami, T. and Tatsumisago, M., *J. Ceram. Soc. Japan*, Suppl., Vol. 112, pp. S1425–S1429 (2004).
37) Matsuda, A., Matoda, T., Kogure, T., Tadanaga, K., Minami, T. and Tatsumisago, M., *J. Sol-Gel Sci. Technol.*, Vol. 31, pp. 229–233 (2004).
38) Matsuda, A., Matoda, T., Kogure, T., Tadanaga, K., Minami, T. and Tatsumisago, M., *Chem. Mater.*, Vol. 17, pp.749–752 (2005).
39) Matsuda, A., Kobayashi, K., Kogure, T., Sakai, M., Tadanaga, K., Minami, T. and Tatsumisago, M., *J. Ceram. Soc. Japan*, Vol. 113, pp. 519–524 (2005).
40) Sasaki, T., Watanabe, M., Michiue, Y., Komatsu, Y., Izumi, F. and Takenouchi, S., *Chem. Mater.*, Vol. 7, pp. 1001–1007 (1995).
41) Sasaki, T., Ebina, Y., Kitami, Y., Watanabe, M. and Oikawa, T., *J. Phys. Chem. B*, Vol. 105, pp. 6116–6121 (2001).
42) Waychunas, G. A., "Structure, Aggregation and Characterization of Nanoparticles in Reviews in Mineralogy and Geochemistry 44," Mineralogical Society of America, Washington DC (2001).
43) Sasaki, T., Komatsu, Y. and Fujiki, Y., *Chem. Mater.*, Vol. 4, pp. 894–899 (1992).
44) Feist, T. P. and Davis, P. K., *J. Solid State Chem.*, Vol. 101, pp. 275–295 (1992).
45) Sasaki, T., Nakano, S., Yamauchi, S. and Watanabe, M., *Chem. Mater.*, Vol. 9, pp. 602–608 (1997).
46) Sasaki, T., Ebina, Y., Tanaka, T., Harada, M., Watanabe, M. and Decher, G., *Chem. Mater.*, Vol. 13, pp. 4661–4667 (2001).
47) Yin, S., Uchida, S., Fujishiro, Y., Aki, M. and Sato, T., *J. Mater. Chem.*, Vol. 9, pp. 1191–1195 (1999).
48) Yanagisawa, M., Uchida, S., Yin, S. and Sato, T., *Chem. Mater.*, Vol. 13, pp. 174–178 (2001).
49) Tadanaga, K., Katada, N. and Minami, T., *J. Am. Ceram. Soc.*, Vol. 80, pp. 1040–1042 (1997).
50) Tadanaga, K., Katada, N. and Minami, T., *J. Am. Ceram. Soc.*, Vol. 80, pp. 3213–3216 (1997).
51) Tadanaga, K., Kitamuro, K., Morinaga, J., Kotani, Y., Matsuda, A. and Minami, T., *Chem. Lett.*, Vol. 2000, pp. 864–865 (2000).
52) Tadanaga, K., Kitamuro, K., Matsuda, A. and Minami, T., *J. Sol-Gel Sci. Technol.*, Vol. 26, pp. 705–708 (2004).
53) Tadanaga, K., Morinaga, J., Matsuda, A. and Minami, T., *Chem. Mater.*, Vol. 12, pp. 590–592 (2000).
54) Penn, R. L. and Banfield, J. F., *Science*, Vol. 281, pp. 969–971 (1999).
55) Penn, R. L. and Banfield, J. F., *Geochimica et Cosmochimica Acta*, Vol. 63, pp. 1549–1557 (1999).
56) Banfield, J. F., Welch, S. A., Zhang, H., Ebert, T. T. and Penn, R. L., *Science*, Vol. 289, pp. 751–754 (2000).
57) Kavan, L., O'Regan, B., Kay, A. and Gartzel, M., *J. Electroanal. Chem.*, Vol. 346, pp. 291–307 (1993).
58) Matsumoto, Y., Ishikawa, Y., Nishida, M. and Ii, S., *J. Phys. Chem. B*, Vol. 104, pp. 4204–4209 (2000).
59) Lei, Y., Zhang, L. D. and Fan, J. C., *Chem. Phys. Lett.*, Vol. 338, pp. 231–236 (2001).
60) Grimes, C. A., Sigh, R. S., Dickey, E. C. and Varghese, O. K., *J. Mater. Res.*, Vol. 16, pp. 1686–1693 (2001).
61) Heijman, S. G. H. and Stein, H. N., *Langmuir*, Vol. 11, pp. 422–427 (1995).
62) Yang, J., Mei, S. and Ferreira, J. M. F., *J. Colloid Inter. Sci.*, Vol. 260, pp. 82–88 (2003).